Use of Data Assimilation for Inference of CA1 Neuron Pathology in 3xTG Mouse Model of Alzheimers

Daniel Breen

November 29, 2016

Abstract

1 Introduction

Alzheimer's is presently diagnosed at the level of behavior at the late stages of the disease, when irreversible cognitive impairment has already occurred. What is now lacking in the understanding of neuropathology are the links between underlying causes at the molecular, single cell, and circuits level of the disease and the behavioral symptoms. Computational modeling offers the potential to link across the different levels of genes and drugs, synapses and neurons, and cognition and behavior to provide a unified, testable basis for formulating therapeutic strategies [4].

Biophysical neuron models such as conductance based Hodgkin Huxley (HH) type models contain interpretable and biologically meaningful parameters capable of reproducing experimentally observed membrane dynamics. Such models thus provide a framework in which to identify changes in biophysical properties of diseased cells in a manner that elicits targets for potential therapeutic intervention.

We wish to identify quantitative changes in the detailed electrical membrane dynamics between wild type and diseased cells where the latter have been genetically modified (in mice) to produce analogs to human Alzheimer's responses. The goal is to further develop HH like models of cortical cells implicated in Alzheimer's disease and to inform the use of well designed experiments which will quantify changes in the intracellular Ca^{2+} dynamics of these cells. Ca^{2+} dynamics has been identified as a target mechanism where early onset of Alzheimer's can be tracked and where further degeneration of healthy cellular behavior can be potentially identified and treated.

We have previously developed methods of statistical data assimilation which have been successful in incorporating information in complex chaotic and neural systems, from incomplete data sets [11, 8, 1, 7, 9, 14, 13].

Other methods of parameter fitting in neuron systems have yielded the estimation of many states and parameters as well, but with one or more of the following limitations:

- parameter identifiability issues are not addressed
- the parameters must be heavily constrained, reflecting unlikely prior knowledge
- only parameters which enter the model linearly can be accurately estimated
- make adequate "best fits" but fail to predict

The first and last are crucial shortcomings - work in single neuron modeling often does not raise the issue about the uniqueness of estimated parameters[2], nor does it often consider the subjectivity of a good fit. These are often tested by eye or may incorporate some heuristic metric of error from the data and will often have poor predictive power.

The approach advanced here directly addresses the issue of testable model fitting in neural systems. Previously, it has demonstrated success in estimating all of the parameters in HH conductance models, including those that enter nonlinearly such as the gating kinetics describing the ion currents. They have also been shown capable of predicting [11, 8, 7, 9, 6] precise waveform information of the voltage of a neuron evolving in time according to a novel stimulating current.

Computational models capable of being rigorously validated by the methods discussed and data that is available must also incorporate enough biological realism to be useful tools in the neuropharmacological process of drug design, such as by prescreening a number of compounds for bench testing in the laboratory. Computational modeling makes explicit simplifying assumptions that all scientists make implicitly, so continuous testing against experimental results is required to inform the use of the model and to ensure that it is accurate.

2 Methods

2.1 CA1 Neuron Model

We found, after subjecting different models to our methods of parameter estimation, that the basic HH model best balances the competing demands of parameter identifiability and biological realism which could account for different features of the data. The basic HH model did better at reproducing these features without the parameter identification issues of more complicated models.

Our CA1 neuron model is thus a basic Hodgkin-Huxley (HH) neuron with only sodium (I_{Na}) and potassium (I_K) currents:

$$C_m \frac{dV(t)}{dt} = g_{Na} m(t)^3 h(t)(E_{Na} - V(t)) + g_K n(t)^4 (E_K - V(t)) \quad (1)$$
$$+ g_L(E_L - V(t)) + I_{injected}(t)$$
$$\frac{dx(t)}{dt} = \frac{x_\infty(V) - x(t)}{\tau_x(V)}$$
$$x_\infty(V) = 0.5(1 + \tanh(\frac{V - \theta_x}{\sigma_x}))$$
$$\tau_x(V) = t_{x0} + t_{x1}(1 - \tanh^2(\frac{V - \theta_x}{\sigma_{xt}})) \quad (2)$$

Here $V(t)$ is the membrane voltage, C_m is the membrane capacitance, and $I_{injected}(t)$ is a known stimulating current injected into the neuron in a current clamp setup. g_i and E_i denote the maximum conductance and reversal potential for current i, respectively.

The equations for x are a shorthand for the kinetics of the gating variables m, h, and n. $x_\infty(V)$ is the voltage dependent steady state activation which depends on θ_x, the voltage at half activation, and σ_x, the width of this activation. $\tau_x(V)$ is the voltage dependent relaxation time, describing the rate that the gating variables change to their steady state values.

A more complex model including more ionic currents would have the advantage of incorporating some elements of biological realism. However, we are interested in estimating parameters and detecting features to distinguish populations of neurons in a biophysical context, so we must take into consideration the parameter identification problem. In our experiments collecting voltage data, we use a current clamp setup, where voltage traces are measured with a known injected current. One example of parameter unidentifiability is that different depolarizing and repolarizing currents can contribute to the opening and closing of ion channels underlying voltage response to injected current. Using only measured voltage, it is hard to say what the relative contributions of different ionic currents could be to characteristics of features like action potentials.

Errors in the descriptions of the dynamics of these channels in HH models and noisy measurements contribute to the parameter identifiability problem. We show, using our data assimilation algorithm described in section 2.2, that we can find sets of parameters in a basic HH model capable of reproducing nearly exactly the shape of the waveform of our recorded data. Correctly predicted features include the shape of the action potential waveform, afterhyperpolarization effects, refractory periods, spike timing, and subthreshold variations.

Our strategy here is to estimate ensembles of models and look for similarities and differences in patterns in these ensembles across distinct populations of neurons. Since there are many sets of model parameters which are compatible with the observed data, we do not attempt to pinpoint a 'correct set' of model parameters.

We do retain some element of subjectivity in that estimated models are said to be compatible with the data when predictions, generated by integrating the

model beyond the estimation, are judged to match the subthreshold voltage variations and spike timing. This subjective evaluation was generally easy as matches to the data were either very good or very poor.

This validation procedure is easily scalable as the process was automated by checking the value of a few features at the end of the data assimilation procedure, including using a spike sorting algorithm which checked whether the prediction contained action potentials with a size within a biologically realistic range (no more than several ms) and whether the value of the objective function, defined in section 2.2, was smaller than a cutoff value.

It is therefore not necessary to check each prediction manually, only to check that the automated process is working sensibly by checking a subsample of the accepted and rejected predictions.

2.2 Methods of Data Assimilation

Data assimilation refers to analytical and numerical procedures in which measurements and models are combined to infer knowledge about a system which is not available in the measurements alone. The problem is typically formulated as follows. We formulate a model describing the system with state variables $\mathbf{x}$ defined at times $t_0, t_1, ..., t_T$, and we seek to infer the model state variables at the end of the estimation window $\mathbf{x}(t_T)$ and the unknown model parameters $\mathbf{p}$.

One of the difficulties commonly encountered in data assimilation arises from the fact that systems in the real world almost always contain processes that the modeler is ignorant about or cannot represent. Another difficulty comes from the fact that measurements are noisy which limits the ability to infer properties of systems even in the presence of perfect models. Estimating properties of the dynamics of systems which are nonlinear, such as neurons, only compounds these problems. Previously, we have developed methods of data assimilation capable of dealing with gaussian measurement noise when the neural system under study is perfectly described by a basic HH model [11, 8, 7]. As our focus here is on data from real neurons, we cannot hope to have a perfect model, but these studies provide a firm basis on which to build our understanding here.

Elsewhere [1, 14, 13, 6], we have applied a data assimilation method we call annealing to arrive at estimates of parameters and unknown states, which involved asking what the configuration of the states and parameters of the system were at the end of an estimation window given a set of observations. We formulate a path integral expression and expand the conditional probabilities within the integral as gaussian measurement noise and model error processes. This formulates the inference problem into an optimization problem, whereby systematically changing the variance over a sequence of annealing steps we could use educated guesses about the location of the best minima of our cost function to enforce both the data and the model and infer an estimated set of parameters describing our system.

Through trial and error, we have determined that another variational approach for formulating the inference problem as an optimization problem may be faster and more robust for inferring unknown states and parameters in single

neuron systems. This method was previously used successfully for estimating models of neurons, using data from neurons in region hvc of the avian song system, in [9] and remains a reliable choice in simpler models, including our basic HH model of CA1 neurons here. A critical concern in variational approaches to nonlinear dynamical systems is that the familiar least-squares objective function may give an irregular search surface with many local minima. We addressed this problem here by including a balanced synchronization term, $u(t)(V_{data}(t) - V(t))$, in the model dynamics, which regularizes and minimizes the influence of local minima by ensuring that the solution set defines a model that is capable of synchronizing with the data. The objective function includes a penalty for this regularization and is taken as

$$\sum_{i=1}^{T}(V_{data}(t) - V(t))^2 + u(t)^2 \tag{3}$$

where $V_{data}(t)$ is the measured voltage, $V(t)$ is the voltage output from the model, and T is the number of discretely sampled time points in the estimation window.

The neuron model that we investigated is not known to be chaotic for the biophysical range of our parameters, but it is nonlinear, and in the high-dimensional search space, there may well exist chaotic regions that must be explored by the optimization routine, and these will benefit from this regularization. Provided a solution to the model can be found that is consistent with the data, at the end of the optimization, the value for the control parameter $u(t)$, describing the magnitude of the synchronization term, should be small relative to the model dynamics. The quality of the model was tested by setting $u(t)$ to zero and integrating the model forward from the end of the assimilation period using the estimated parameter and state values.

The implementation of the data assimilation algorithm was accomplished through the use of the open source software package IPOPT (Interior Point OPTimizer) with the linear solver ma57 [12].

2.3 Detecting Altered Features and Mechanisms

We are interested in identifying features in our models which are different in 3xTG neurons. Using the estimated models, the number of features was expanded from the set of 20 estimated parameters in the models to include the about 100 total features of Table 9 in section 5, including the spike half-width of model predictions obtained by integrating the model forward past the end of the estimation window. The predictions are the red traces such as those shown in Figure 1.

We trained random and regression forest models using the features of Table 9 to predict labels of interest, including the known type of each neuron (3xTG or healthy), threshold voltage, and spike half-width. We used a feature importance evaluation to determine the relative importance of each feature in predicting each label.

Feature importances significantly reduce the number of feature subspaces to examine when manually searching for predictive features, such as looking for differences between the two populations of neurons.

We display correlations between features detected to be altered in 3xTG neurons and model parameters proposed to act as mechanisms causing these differences. We also show decision and regression trees which give a more nuanced understanding of the structure of the estimated ensemble in the high dimensional feature and parameter space.

Each recorded data set differed in the quality of the estimated models, as judged by the accuracy of the predictions. It was not necessary to keep all epochs in the data set to draw out the differences between properties of the healthy and 3xTG neurons. We therefore discarded a few of the 21 epochs of the data set in the rest of the analysis to include only the best predictions. However, because the sample size of neurons is small, with two 3xTG and three healthy neurons studied, any conclusions we draw about the differences between the two populations is tentative.

3 Results

3.1 Estimating Ensembles of Models

Using our methods of data assimilation, we estimated model parameters for 21 measured voltage waveforms generated using one of a few known, complex, injected currents. For each data set, we initialized our data assimilation search procedure with 500 distinct sets of parameters sampling each parameter from a uniform distribution defined between the parameter bounds.

Much of the power of this analysis derives from the data assimilation procedure described in 2.2 and elsewhere. When integrated forward, the estimated models accurately predict spike timing, subthreshold variation, afterhyperpolarization, spike amplitude and other features within the range of biological trial by trial variability. This even holds true with a basic HH model with only the usual I_{Na} and I_K currents, despite missing many other currents which are present. Exemplars of this data assimilation protocol on the data set are displayed in Figure 1.

3.2 Identifying Differences Between 3xTG and Healthy Neurons

3.2.1 Differences in Passive Membrane Properties

Including the full set of features of Table 9, we find from Table 1 that spike half-width, g_L, and C_m are the features with the largest variable importances for distinguishing between the two populations. From the raw voltage traces, 3xTG neurons have a larger average spike half-width (2.7 ms) than healthy cells (2.0 ms), which is consistent with findings elsewhere [10].

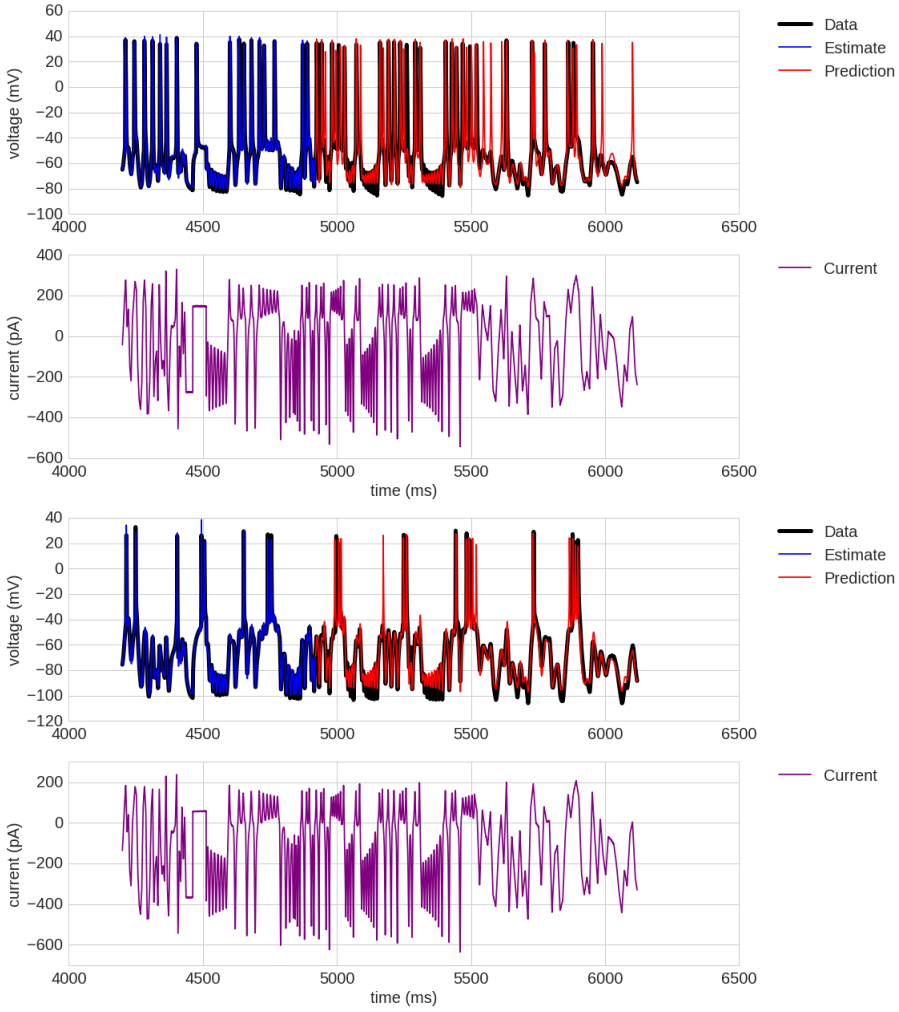

Figure 1: Estimated voltage (blue), stimulating current (purple), data (bold black), and prediction (red), obtained by integrating the estimated model forward in time, shown for a 3xTG neuron (top) and a healthy neuron (bottom). The stimulating current waveform used in the data assimilation procedures is a combination of pseudo-noisy currents and the output of a chaotic model. The pseudo-noisy currents were created by uniformly sampling current values about every 20 ms and linearly interpolating in between. The chaotic current waveform is the output from the Lorenz63 model used as a stimulating current.

All Features Predicting Type	Var Imp	Features C_m and g_L Excluded	Var Imp
half-width (ms)	0.118	half-width (ms)	0.151
g_L (nS)	0.080	Max $\dot{I}_{Na}$ Upstroke (pA/ms)	0.053
C_m (pF)	0.066	t_{h0} (ms)	0.044
Max $\dot{I}_{Na}$ Upstroke (pA/ms)	0.045	θ_h (mV)	0.043
θ_h (mV)	0.037	Max $\dot{g}_{Na}$ Upstroke (nS/ms)	0.036
Max $\dot{g}_{Na}$ Upstroke (nS/ms)	0.031	g_K (nS)	0.031
E_L (mV)	0.028	Max I_{Na} Upstroke (pA)	0.031
Max g_{Na} Downstroke (nS)	0.026	Δ_{mh} (ms)	0.026
Voltage at Max I_{Na} Downstroke (mV)	0.022	Max g_{Na} Upstroke (nS)	0.023
Max I_{Na} Upstroke (pA)	0.021	Voltage at Max I_{Na} Downstroke (mV)	0.023
Δ_{mh} (ms)	0.021	Voltage at Min $\dot{I}_{Na}$ Downstroke (mV)	0.022
Voltage at Max $\dot{I}_{Na}$ Downstroke (mV)	0.020	Max g_{Na} Downstroke (nS)	0.021
t_{h0} (ms)	0.019	E_L (mV)	0.020
Voltage at Max g_{Na} Upstroke (mV)	0.019	threshold step current (pA)	0.020
Threshold $\dot{g}_{Na}$ Upstroke (nS/ms)	0.018	Voltage at Max g_{Na} Upstroke (mV)	0.019
Threshold $\dot{I}_{Na}$ Upstroke (pA/ms)	0.018	Threshold $\dot{g}_{Na}$ Upstroke (nS/ms)	0.018
threshold step current (pA)	0.017	threshold voltage (mV)	0.017
g_K (nS)	0.017	Min $\dot{I}_{Na}$ Upstroke (pA/ms)	0.017
Min $\dot{I}_K$ Downstroke (pA/ms)	0.016	Min $\dot{I}_K$ Downstroke (pA/ms)	0.014
Voltage at Min $\dot{I}_{Na}$ Downstroke (mV)	0.015	Voltage at Max g_K Upstroke (mV)	0.014

Table 1: Feature Importance Table. The left two columns are the importance calculated from a random forest classifier trained on the full set of features, while the right two columns are trained on a subset excluding C_m and g_L. These two parameters are excluded because it is not clear from Figure 2 that they distinguish between 3xTG and healthy neurons, although the scatter is suggestive. Features measuring half width, timing of I_{Na} and I_K, and excitability are the most important distinguishing characteristics.

All Params Predicting Type	Var Imp	Params C_m and g_L Excluded	Var Imp
g_L (nS)	0.236	θ_h (mV)	0.149
C_m (pF)	0.128	t_{h0} (ms)	0.131
E_L (mV)	0.091	g_K (nS)	0.085
θ_h (mV)	0.083	σ_{ht} (mV)	0.080
t_{h0} (ms)	0.076	E_L (mV)	0.071
g_K (nS)	0.063	t_{m0} (ms)	0.053
θ_n (mV)	0.038	t_{m1} (ms)	0.047
σ_{ht} (mV)	0.037	σ_m (mV)	0.046
σ_h (mV)	0.029	t_{n0} (ms)	0.045
t_{m1} (ms)	0.026	t_{h1} (ms)	0.043
σ_m (mV)	0.025	σ_h (mV)	0.043
t_{n0} (ms)	0.025	θ_n (mV)	0.041
t_{h1} (ms)	0.023	θ_m (mV)	0.037
θ_m (mV)	0.021	g_{Na} (nS)	0.029
σ_n (mV)	0.020	σ_{nt} (mV)	0.028
t_{m0} (ms)	0.020	σ_n (mV)	0.026
t_{n1} (ms)	0.019	t_{n1} (ms)	0.025
σ_{nt} (mV)	0.016	σ_{mt} (mV)	0.021

Table 2: Feature importance calculated using a subset of the features of Table 1, the model parameters alone. From Table 1, spike half-width and certain measures of excitability are important. This table suggests that the rate of inactivation of h at voltages far away from threshold, where that threshold occurs, and the strength of I_K are important in distinguishing 3xTG and healthy neurons.

We show in the scatterplot of Figure 2 C_m against g_L to observe how values of these quantities are distributed in the ensemble. We find that although C_m and g_L tend to produce clusters in the healthy neurons studied, it appears there are two clusters in the 3xTG neurons.

A larger resting membrane conductance in 3xTG neurons is consistent with the idea that I_L may be larger due to the integrity of the cell membrane being compromised, but it is not clear why the membrane capacitance would be larger in 3xTG neurons, so C_m, as well as other features, may be spuriously estimated to be different in each population due to the small sample size, such as from one of the 3xTG neurons having a coincidentally larger membrane capacitance.

There also does not seem to be a full separation between categories in the (C_m, g_L) subspace, so we also display in Table 1 the variable importances when these features are omitted from the random forest model.

Increased excitability is reported [3, 5] in 3xTG neurons. We also find increased excitability here, in the sense of a lowered threshold step current and threshold voltage required to elicit an action potential in 3xTG cells. We find also E_L estimated to be larger, with an increased leak current I_L apparent in the (E_L, g_L) subspace of Figure 4. There is a close relationship between lowered threshold applied current and threshold voltage which is shown in Figure 3.

The feature importance associated with E_L is a little more subtle. Excitability can be defined in a number of different ways. Increasing E_L is equivalent to applying a constant positive current to the neuron. This tends to lower the step current associated with generating an action potential and counteracts repolarizing currents such as I_K. E_L tends to be larger in one of the 3xTG cells than in the healthy cells, but not in the other. However, in both 3xTG cells, I_L has a larger magnitude. The 3xTG cell in which a difference in C_m and g_L is not seen (Figure 2) separates out in the (E_L, g_L) subspace (Figure 4).

Based on the findings that half-width and excitability help to differentiate 3xTG and healthy neurons, we are not surprised to find the good separation in a subspace containing the threshold step current and spike half-width of Figure 5.

3.2.2 Mechanisms Underlying Differences in Threshold Voltage

So far, we have mainly discussed the differences in the passive membrane properties between the two categories of cells.

Differences in the way I_{Na} and I_K are involved in action potentials is suggested by Tables 1 and 2. For example, the maximum value of g_{Na} on the upstroke of an action potential and the voltage at which the maximum value of I_{Na} occurs both have high variable importance in differentiating 3xTG and healthy neurons. These in turn depend on factors like the magnitude and timing of I_{Na} and I_K.

θ_h, σ_h, θ_m, and σ_m help to define the threshold voltage of a neuron. θ_m describes the voltage at which the state variable $m(t)$ describing $I_{Na}(t)$ reaches half of its maximum value. σ_m describes the width at which this transition occurs, as can be seen by examining Equation 1.

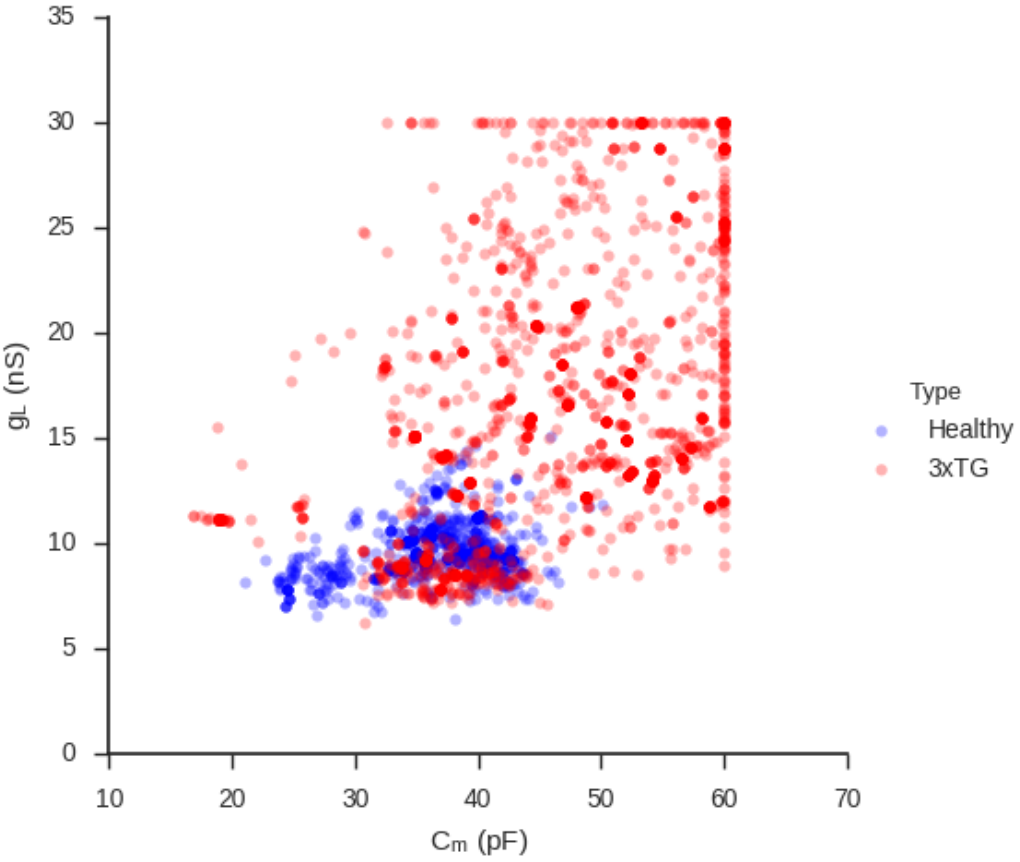

Figure 2: Scatter in the (C_m, g_L) subspace, with 3xTG estimated values plotted in red, healthy cells in blue. There is a separation in a subset of the estimated values in both dimensions, but not another. When other dimensions, such as E_L are also included as in Figure 4, all of the 3xTG values are better separated out from the healthy ones.

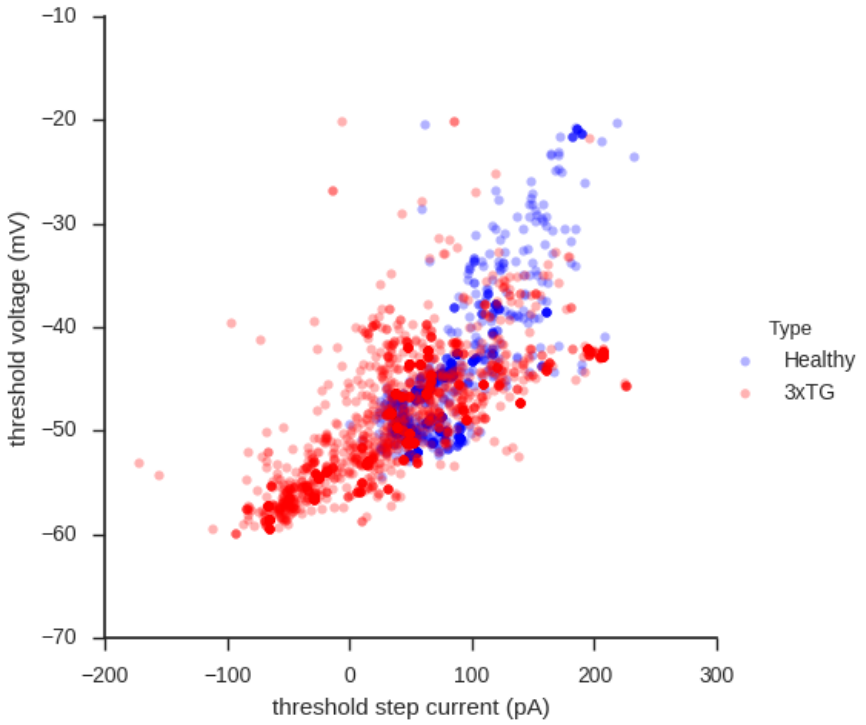

Figure 3: The minimum applied step current required to elicit an action potential plotted against the corresponding threshold voltage determined in this manner. An action potential is defined by a membrane voltage exceeding 5 mV. Many of the estimated 3xTG models separate from the healthy cell models in this subspace.

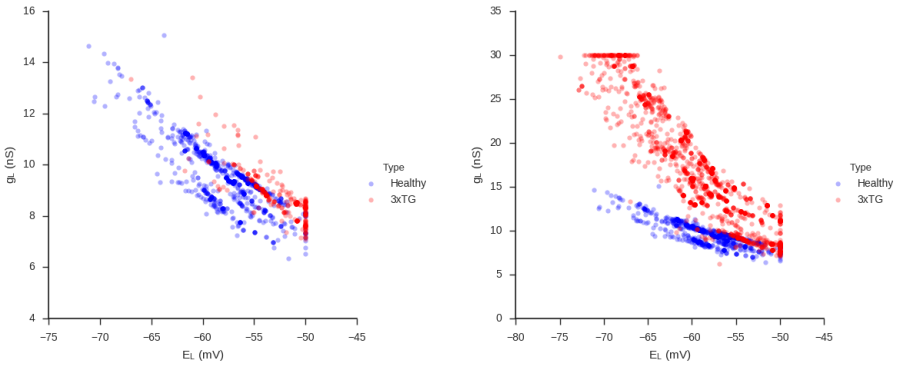

Figure 4: Right: E_L plotted against g_L for the ensemble of estimated models using all neurons. The scatter in the (E_L, g_L) subspace shows that I_L is larger in 3xTG cells. E_L is larger in 3xTG cells. which is equivalent to a constant relatively positive applied current. Left: When only values from one 3xTG are plotted in red along with all healthy values in blue, E_L and g_L are still related to each other.

$m(t)$ must change more quickly in time than $h(t)$ in order for an action potential to be generated. If $h(t)$ inactivates I_{Na} prematurely, no action potential will be generated. Because of this, and since θ_h simultaneously describes the voltage at which the steady state value of h and its relaxation time change, both θ_m and θ_h tend to be estimated in a range around the threshold voltage. Since the threshold voltage is estimated to be different in the two classes of neurons (Figure 3), we expect differences in θ_h, σ_h, θ_m, and σ_m in the two classes of neurons.

θ_m and σ_m have modest importances individually compared to the features discussed above, but in two dimensions (Figure 6) a separation between 3xTG and healthy cells is apparent and provides evidence that altered kinetics in I_{Na} results in a lower threshold voltage in 3xTG. It also helps to explain the dependence of threshold voltage on threshold current of Figure 3.

Therapeutic remedies could be screened in one way by checking for whether they can shift the value of θ_m and/or σ_m in 3xTG cells into the healthy regime of Figure 6.

We can use regression forests to discover features which are important in predicting properties associated with excitability, such as threshold voltage and the associated threshold current.

θ_h, θ_m, and E_L have high importance when predicting threshold voltage in Table 4, confirming our intuitions of about these parameters. Alongside the feature importance values, we include also the correlation between threshold voltage and each of the predicting features. We note here that C_m and g_L tend to appear as predictors in our regression analyses, but the relationship here seems likely to be correlation rather than causation, so they are omitted

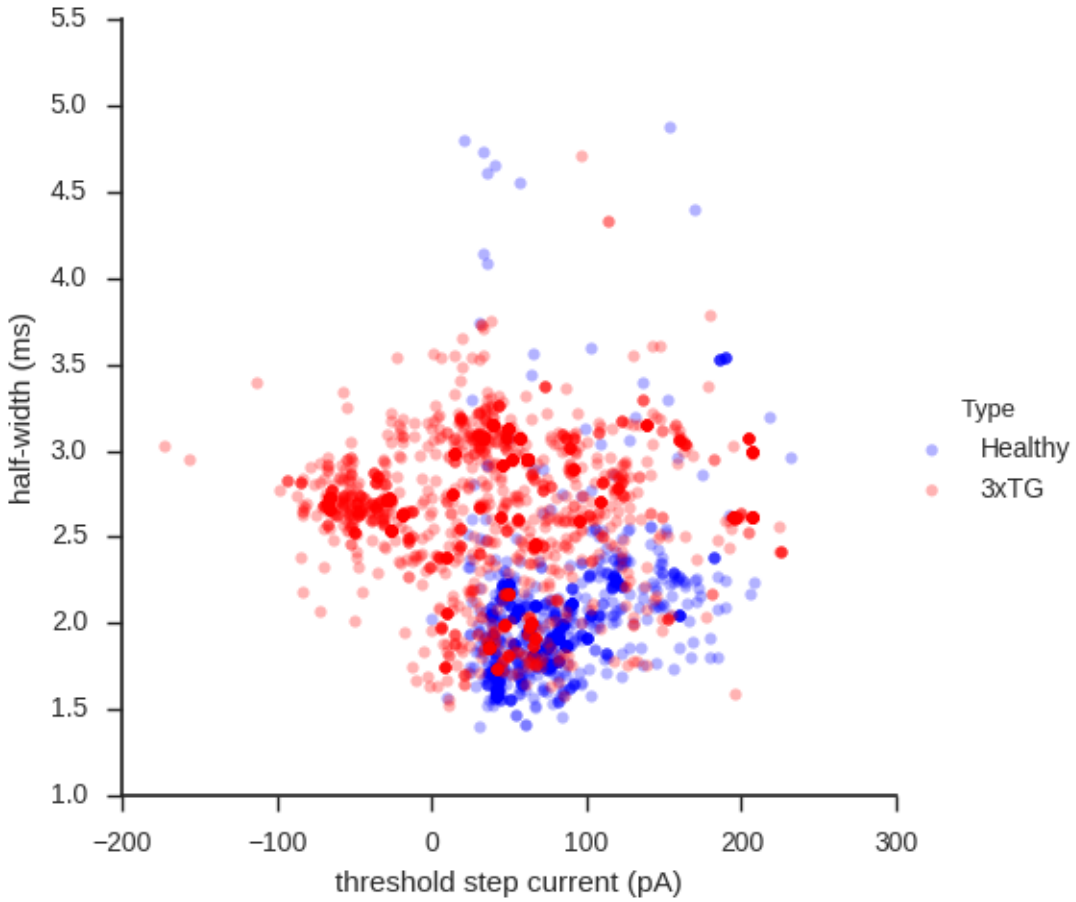

Figure 5: The high variable importance of features associated with excitability and spike width motivate looking at the separation of classes in such a subspace. We find good separation between the two classes.

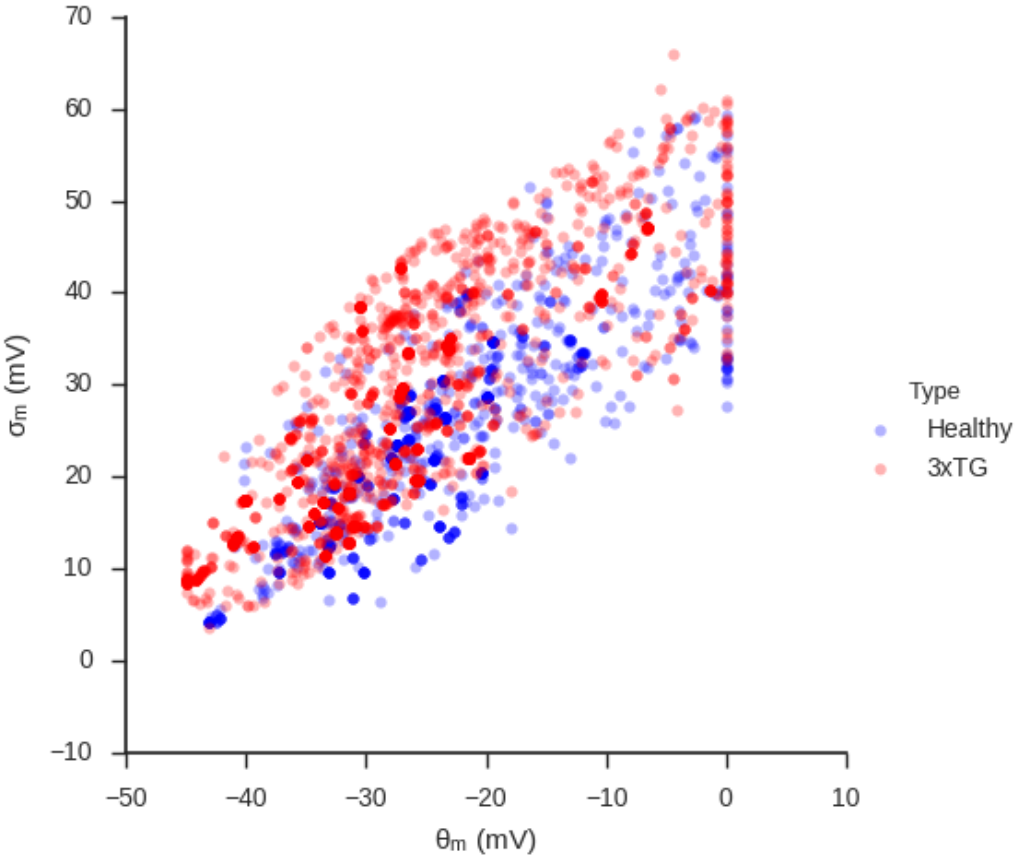

Figure 6: Although θ_m and σ_m each have modest importances according to Table 2, in two dimensions the separation between the two classes of neurons becomes much more apparent.

Features Predicting Threshold Voltage	Var Imp	Correlation
Voltage at Max $\dot{I}_{Na}$ Upstroke (mV)	0.334	0.252
Threshold $\dot{I}_K$ Upstroke (pA/ms)	0.131	-0.195
Max I_{Na} Upstroke (pA)	0.099	-0.366
E_L (mV)	0.061	0.259
Max g_{Na} Upstroke (nS)	0.048	-0.280
Threshold g_{Na} Upstroke (nS)	0.042	0.417
Threshold $\dot{g}_{Na}$ Upstroke (nS/ms)	0.027	0.191
Max $\dot{I}_{Na}$ Upstroke (pA/ms)	0.023	-0.295
Min $\dot{I}_{Na}$ Upstroke (pA/ms)	0.022	0.351
Max g_{Na} Downstroke (nS)	0.021	-0.189
Max $\dot{g}_{Na}$ Upstroke (nS/ms)	0.020	-0.197
Threshold $\dot{I}_K$ Downstroke (pA/ms)	0.019	0.287
Max I_{Na} Downstroke (pA)	0.014	-0.136
θ_n (mV)	0.014	-0.139
θ_h (mV)	0.013	0.259
Δ_{mh} (ms)	0.010	-0.181
θ_m (mV)	0.010	0.326
σ_m (mV)	0.007	0.014
Min $\dot{g}_{Na}$ Downstroke (nS/ms)	0.006	0.124
Max $\dot{I}_K$ Downstroke (pA/ms)	0.005	-0.067

Table 3: Feature importances for threshold voltage calculated from a regression forest trained on the ensemble of models. The voltage at max $\dot{I}_{Na}$, among the most important features, is closely related to θ_m, with Table 4 bolstering evidence for this claim. θ_m is the voltage at which the activation variable m changes most rapidly. Also important is $\dot{I}_K$, the rate at which I_K turns on with respect to time, at threshold voltage. g_L and C_m may simply be correlated with threshold voltage.

as variables.

The voltage where $\dot{I}_{Na}$ is maximum is related to θ_m, as the upswing in voltage during an action potential is primarily due to I_{Na}, and the activation variable m is changing most rapidly around the voltage θ_m. There are other features which are more highly correlated with threshold voltage such as g_{Na} at threshold voltage, but in a decision tree structure, at least, $\dot{I}_{Na}$ has more predictive power.

The causes of low threshold step current, from Tables 5 and 6.. , involve the strength of I_{Na} and where this current becomes active. which is related to the threshold voltage. θ_h is one of the best predictors of threshold voltage in Tables 3 and 4, so it is not surprising that it is also a strong predictor for threshold current. We omit the threshold voltage as a predictor in Tables 5 and 6.

All Params Predicting Threshold Voltage	Var Imp	Correlation
θ_h (mV)	0.432	0.263
θ_m (mV)	0.134	0.319
E_L (mV)	0.084	0.254
σ_{ht} (mV)	0.067	-0.211
t_{m1} (ms)	0.046	0.023
θ_n (mV)	0.035	-0.148
σ_h (mV)	0.035	-0.060
σ_m (mV)	0.035	0.015
t_{h1} (ms)	0.029	-0.277
g_{Na} (nS)	0.023	-0.154
g_K (nS)	0.016	-0.168
t_{m0} (ms)	0.014	-0.167
σ_n (mV)	0.013	-0.090
t_{h0} (ms)	0.012	-0.197
σ_{mt} (mV)	0.008	-0.184
t_{n0} (ms)	0.006	-0.057
t_{n1} (ms)	0.005	-0.164
σ_{nt} (mV)	0.004	-0.068

Table 4: Feature importances for threshold voltage using only the model parameters as predictors. In this case g_L and C_m may be correlated with threshold voltage, but θ_h, θ_m, and E_L suggest more mechanistic interpretations.

Features Predicting Threshold Current	Var Imp	Correlation
Max $\dot{I}_{Na}$ Upstroke (pA/ms)	0.340	-0.357
Threshold g_{Na} Downstroke (nS)	0.140	0.284
θ_h (mV)	0.099	0.398
t_{m0} (ms)	0.050	-0.090
Min $\dot{I}_{Na}$ Downstroke (pA/ms)	0.044	0.150
Threshold g_K Upstroke (nS)	0.043	0.370
Max g_{Na} Downstroke (nS)	0.042	-0.297
Max $\dot{g}_K$ Upstroke (nS/ms)	0.031	-0.192
t_{h0} (ms)	0.030	-0.176
Threshold $\dot{I}_K$ Upstroke (pA/ms)	0.020	-0.051
Max I_{Na} Upstroke (pA)	0.017	-0.424
σ_n (mV)	0.011	-0.273
Threshold $\dot{I}_K$ Downstroke (pA/ms)	0.010	0.046
θ_m (mV)	0.007	0.135
t_{m1} (ms)	0.007	-0.023
t_{h1} (ms)	0.007	-0.353
Δ_{mh} (ms)	0.006	-0.169
Threshold g_K Downstroke (nS)	0.006	0.300
Threshold I_K Upstroke (pA)	0.005	0.199
Max I_{Na} Downstroke (pA)	0.005	-0.233

Table 5: Feature importances for threshold step current. Threshold voltage has been omitted as a predictor. The maximum value of $\dot{I}_{Na}$ may be a strong predictor because it encodes the relative strength of I_{Na} as it escapes the regime of threshold voltage.

All Params Predicting Threshold Current	Var Imp	Correlation
θ_h (mV)	0.400	0.406
E_L (mV)	0.125	0.154
θ_m (mV)	0.081	0.136
t_{h0} (ms)	0.075	-0.177
t_{m1} (ms)	0.068	-0.027
σ_m (mV)	0.041	-0.094
σ_{ht} (mV)	0.037	-0.138
t_{h1} (ms)	0.030	-0.343
t_{m0} (ms)	0.024	-0.084
g_{Na} (nS)	0.023	-0.233
g_K (nS)	0.019	-0.191
σ_n (mV)	0.018	-0.267
σ_h (mV)	0.016	0.170
t_{n0} (ms)	0.011	-0.069
θ_n (mV)	0.011	-0.201
σ_{nt} (mV)	0.010	-0.068
σ_{mt} (mV)	0.006	-0.127
t_{n1} (ms)	0.005	-0.121

Table 6: Feature importances for threshold step current using only model parameters. θ_h is a good predictor as it encodes information about where I_{Na} must become active more accurately than any single parameter describing I_{Na}'s kinetics in this region, including g_{Na} and parameters describing m's activation. From Table 4, θ_h is an excellent predictor of the threshold voltage, so it makes sense as a good predictor of threshold current here. E_L is a good predictor since E_L itself acts as a DC current.

Features Predicting Width	Var Imp	Correlation
t_{h0} (ms)	0.363	0.426
Δ_{mh} (ms)	0.102	0.432
Threshold $\dot{I}_K$ Upstroke (pA/ms)	0.082	0.044
σ_{ht} (mV)	0.064	0.225
Max $\dot{I}_{Na}$ Upstroke (pA/ms)	0.053	0.121
Min $\dot{g}_{Na}$ Downstroke (nS/ms)	0.027	-0.011
Min $\dot{I}_{Na}$ Downstroke (pA/ms)	0.027	0.068
Min $\dot{g}_{Na}$ Upstroke (nS/ms)	0.026	0.217
θ_m (mV)	0.021	-0.014
Min I_K Downstroke (pA)	0.016	-0.090
Max g_{Na} Upstroke (nS)	0.014	0.167
Max I_{Na} Upstroke (pA)	0.013	0.123
Min $\dot{I}_K$ Upstroke (pA/ms)	0.012	-0.050
Max $\dot{g}_K$ Upstroke (nS/ms)	0.012	0.051
E_L (mV)	0.012	-0.232
t_{m0} (ms)	0.011	0.001
Max $\dot{g}_K$ Downstroke (nS/ms)	0.010	0.027
Max $\dot{g}_{Na}$ Upstroke (nS/ms)	0.010	0.130
Max g_K Upstroke (nS)	0.009	-0.032
Threshold $\dot{I}_{Na}$ Upstroke (pA/ms)	0.009	-0.013

Table 7: Here again, we can find support for likely underlying mechanisms increasing spike width by using feature importances of regression forests. In this case, we train a regression forest and use a number of features to predict spike width. t_{h0}, the rate of inactivation of h at high voltages, is prominent. Another feature which we find to be highly predictive of spike width is, unsurprisingly, the time duration Δ_{mh} between maximum m and minimum h.

3.2.3 Mechanisms Underlying Differences in Spike Width

Recall from Table 1 that half-width was one of the most important differentiating characteristics between the two classes of neuron. 3xTG neurons exhibit a larger spike width. One mechanism which could cause this involves a decreased value of I_K during action potentials [5], which would cause 3xTG neurons to repolarize more slowly. Another mechanism causing this could be I_{Na} inactivating more slowly.

σ_{ht} describes the width of the voltage dependent relaxation time for h and helps define where the base relaxation time t_{h0} dominates the contribution to t_h.

t_{h0} describes the rate at which I_{Na} is inactivated at high voltages, so we would expect this parameter an important mechanism in increasing spike width. From Table 8, the values of t_{h0} and σ_{ht} have the strongest relationship to the spike half-width of a model. t_{n0} and t_{n1} are also predictive of spike width, as a more slowly activating I_K current will increase spike duration.

All Params Predicting Width	Var Imp	Correlation
t_{h0} (ms)	0.437	0.430
σ_{ht} (mV)	0.112	0.218
t_{n0} (ms)	0.092	-0.012
t_{n1} (ms)	0.082	0.176
θ_m (mV)	0.065	-0.012
g_K (nS)	0.028	0.154
E_L (mV)	0.026	-0.235
σ_h (mV)	0.025	-0.009
θ_h (mV)	0.021	-0.066
σ_{nt} (mV)	0.020	-0.009
θ_n (mV)	0.019	0.219
t_{h1} (ms)	0.018	0.137
g_{Na} (nS)	0.012	0.121
t_{m1} (ms)	0.011	-0.148
σ_m (mV)	0.011	0.140
σ_n (mV)	0.009	0.056
t_{m0} (ms)	0.007	0.011
σ_{mt} (mV)	0.006	0.055

Table 8: We find that parameters associated with timing of I_{Na} and I_K are the most significant predictors of spike width.

3.3 Decision Trees

We can use the first few levels of decision trees to gain more insight into the boundaries in the high dimensional feature space separating 3xTG and healthy neurons. We use the abbreviations defined in the list of features of Table 9, and we build the decision trees without g_L and C_m in case these are not, in reality, useful in discriminating 3xTG and healthy neurons.

When the single decision tree of Figure 7 is trained on the data, spike half-width is the first feature which is used to split the data.

3.3.1 Regression Trees

3.4 Evaluating Therapeutic Remedies

From Tables 7 and 8, variable importances of parameters associated with inactivation of I_{Na}, such as Δ_{mh}, t_{h0}, and σ_{ht} are highest. This is followed by analagous parameters describing the timing of I_K, which may suggest that although these mechanisms may be important, I_{Na} may involve the most significant mechanisms underlying the observed differences in width.

Therapeutic remedies could be evaluated by their ability to restore the excitability of 3xTG cells to healthy values, as measured by estimated values of θ_m and θ_h. We might look for an increase in the average estimate across ensembles of models in θ_m and θ_h by $\approx$ 5-10 mV.

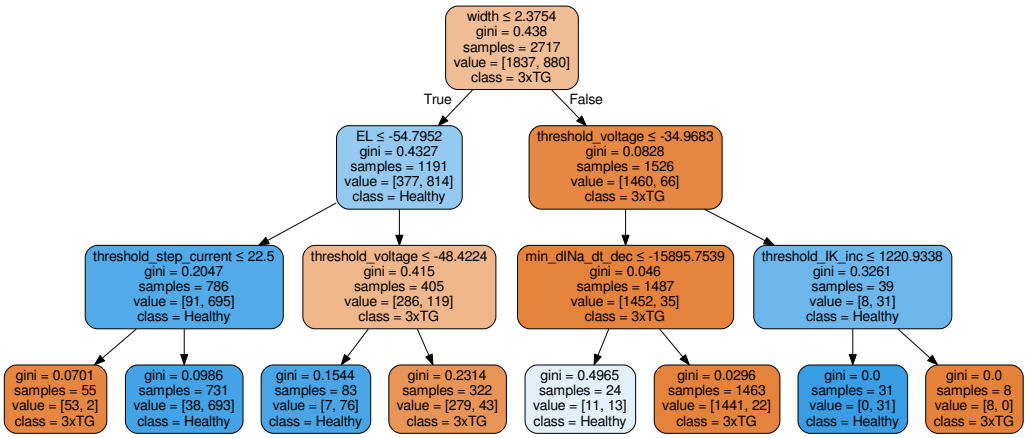

Figure 7: A short decision tree trained on 90% of the training data. The remaining 10% is used to evaluate the ability of the decision tree to generalize on new data (93% accuracy). The color of the fill of the node indicates which class constitutes the majority of samples. Blue nodes are mostly healthy, red are mostly 3xTG. A leftward oriented arrow indicates the node preceding is evaluated to true, rightward false. The structure of the tree suggests that besides width, the excitability of an estimated model is important. This is primarily in two senses, one by the threshold voltage and the second by E_L or the threshold current eliciting an action potential. The meaning of the abbreviations for features in the leaves are in Table 9.

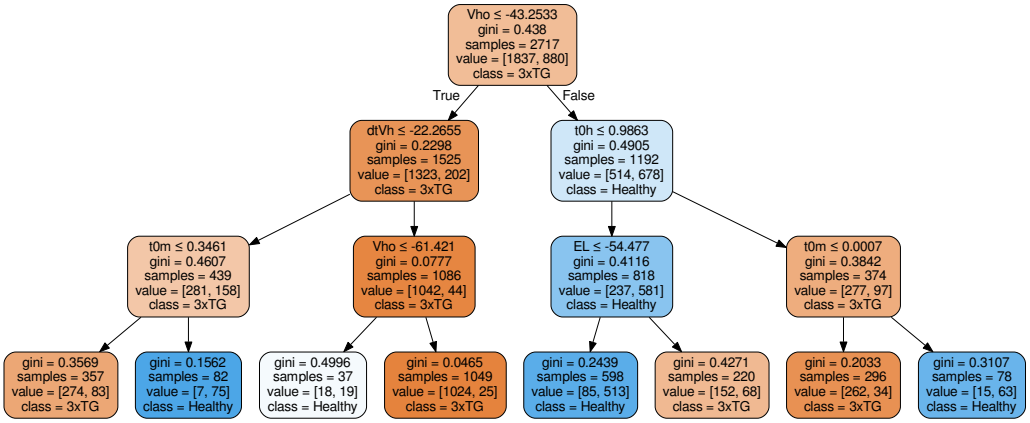

Figure 8: Decision tree analagous to Figure 8, but with only model parameters as predictors. This short tree has 85% accuracy. θ_h (Vho) and E_L are proxies for excitability, while σ_{ht} (dtVh) and t_{h0} (t0h) give information about spike width.

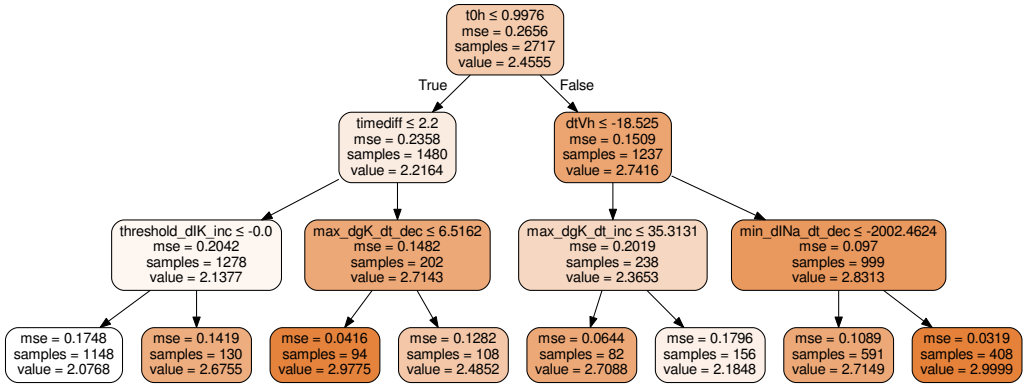

Figure 9: Regression tree predicting width using the full set of features. Inactivation timing information about I_{Na} are most predictive, followed by strength and timing of I_K.

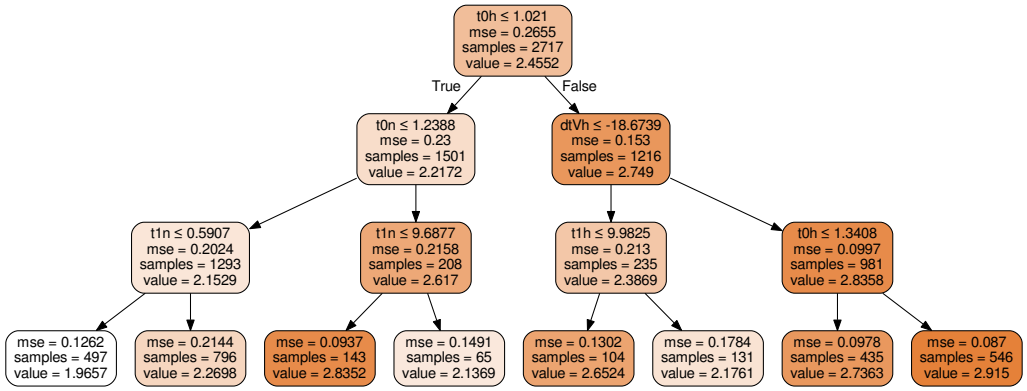

Figure 10: Regression tree predicting width using only estimated model parameters as features. Analagously to Figure 9, timing information about I_{Na} is most important, followed by timing information about I_K

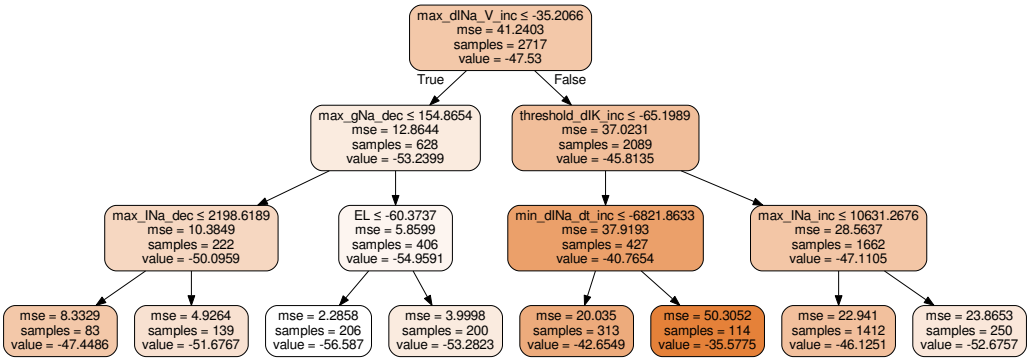

Figure 11: Regression tree predicting threshold voltage using the full set of features. Information about where I_{Na} becomes active is most important, followed by information about I_K and I_L.

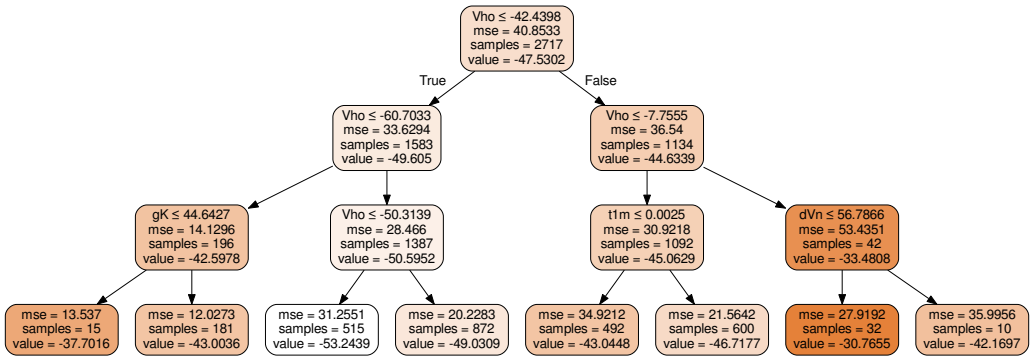

Figure 12: Regression tree predicting threshold voltage using only estimated model parameters. θ_h (Vho) is a good indication about where I_{Na} becomes active, which in turn predicts threshold voltage.

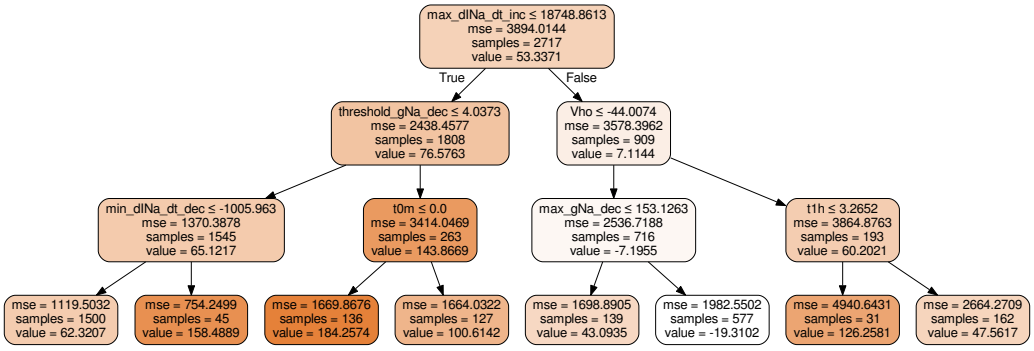

Figure 13: Regression tree predicting threshold current using the full set of features. Information about where I_{Na} becomes active is most important, followed by information about the rate of inactivation of I_{Na} around threshold voltages.

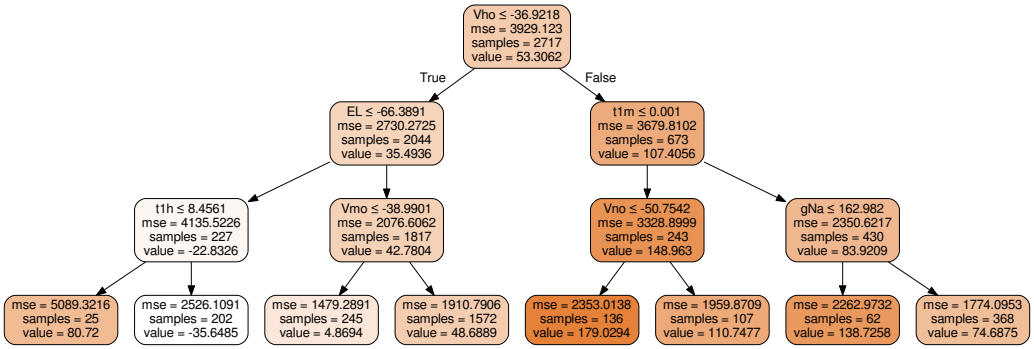

Figure 14: Regression tree predicting threshold step current using only estimated model parameters. Again, information about I_{Na} is most important, followed by information about I_L and I_K.

To restore the spike width of 3xTG cells to healthy values, we might propose decreasing the value of t_h at more positive voltages while ensuring that t_h at lower voltages remains large enough not to preempt action potentials. The results of applying each of these transformations to an exemplar set of estimated parameters of a 3xTG neuron is displayed in Figure 15

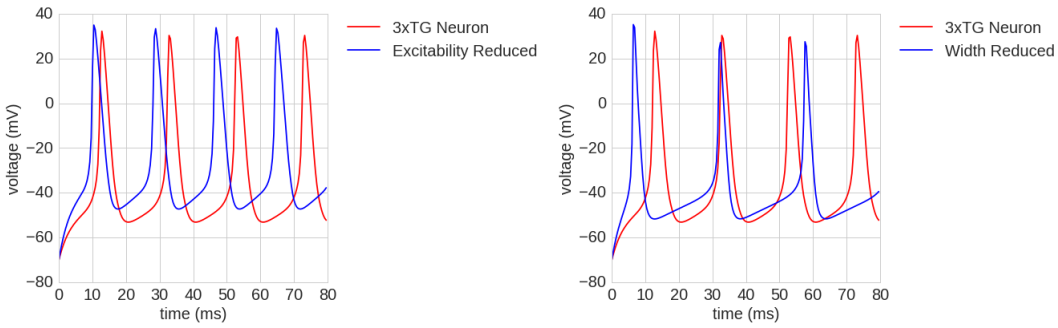

Figure 15: We are interested in decreasing the excitability and spike-width of a 3xTG cell. We integrate our estimated model of a 3xTG neuron forward in time using a step current as a stimulus. We find that if we increase θ_h by 10 (from -46 mV) and θ_m (from -20 mV) by 5 simultaneously (but not independently), we can increase the minimum required step current to produce a spike from about 70 pA to about 270 pA and increase the threshold voltage from about -50 mV to -40 mV. This has no effect on the spike width, however. The simulated action potentials are displayed in the top panel. Next, in addition to the previous modifications, we can also decrease σ_{ht} by 20 mV (from about -3 mV) and decrease t_{h0} (by a factor of four). This decreases the spike width from about 2.76 ms to about 2 ms. It also does lower the minimum required step current to initiate a spike by about 70 pA (to 200 pA), but this is still well within the healthy range for this parameter. Decreasing σ_{ht} to more negative values widens the range at which the inactivation variable h for the sodium current changes slowly. This enables us to decrease the value of t_{h0} overall, which at more positive voltages causes the sodium current to inactivate more quickly, shortening the width of the spike. The net effect on the shape of t_h is to increase its value near voltages important for spike generation so that we don't preempt spikes altogether by decreasing t_{h0}, but to otherwise increase the rate of inactivation during an action potential. Without changing the value of σ_{ht}, we cannot decrease the value of t_{h0} by much.

4 Discussion

5 Feature Abbreviations

Table 9: Predictive features used and their abbreviations.

References

[1] Henry DI Abarbanel. Predicting the future. *AMC*, 10:12, 2013.

[2] Dávid Csercsik, Katalin M Hangos, and Gábor Szederkényi. Identifiability analysis and parameter estimation of a single hodgkin–huxley type voltage dependent ion channel under voltage step measurement conditions. *Neurocomputing*, 77(1):178–188, 2012.

[3] Katherine E Davis, Sarah Fox, and John Gigg. Increased hippocampal excitability in the 3xtgad mouse model for alzheimer's disease in vivo. *PLoS One*, 9(3):e91203, 2014.

[4] Michele Ferrante, Kim T Blackwell, Michele Migliore, and Giorgio A Ascoli. Computational models of neuronal biophysics and the characterization of potential neuropharmacological targets. *Current medicinal chemistry*, 15(24):2456–2471, 2008.

[5] V Frazzini, S Guarnieri, M Bomba, R Navarra, C Morabito, MA Mariggiò, and SL Sensi. Altered kv2. 1 functioning promotes increased excitability in hippocampal neurons of an alzheimer's disease mouse model. *Cell death & disease*, 7(2):e2100, 2016.

[6] Nirag Kadakia, Eve Armstrong, Daniel Breen, Uriel Morone, Arij Daou, Daniel Margoliash, and Henry DI Abarbanel. Nonlinear statistical data assimilation for hvc_ {\ mathrm {RA}} neurons in the avian song system. *Biological Cybernetics*, pages 1–18.

[7] Chris Knowlton, C Daniel Meliza, Daniel Margoliash, and Henry DI Abarbanel. Dynamical estimation of neuron and network properties iii: network analysis using neuron spike times. *Biological cybernetics*, 108(3):261–273, 2014.

[8] Mark Kostuk, Bryan A Toth, C Daniel Meliza, Daniel Margoliash, and Henry DI Abarbanel. Dynamical estimation of neuron and network properties ii: path integral monte carlo methods. *Biological cybernetics*, 106(3):155–167, 2012.

[9] C Daniel Meliza, Mark Kostuk, Hao Huang, Alain Nogaret, Daniel Margoliash, and Henry DI Abarbanel. Estimating parameters and predicting

membrane voltages with conductance-based neuron models. *Biological cybernetics*, 108(4):495–516, 2014.

[10] Federico Scala, Salvatore Fusco, Cristian Ripoli, Roberto Piacentini, Domenica Donatella Li Puma, Matteo Spinelli, Fernanda Laezza, Claudio Grassi, and Marcello D'Ascenzo. Intraneuronal aβ accumulation induces hippocampal neuron hyperexcitability through a-type k+ current inhibition mediated by activation of caspases and gsk-3. *Neurobiology of aging*, 36(2):886–900, 2015.

[11] Bryan A Toth, Mark Kostuk, C Daniel Meliza, Daniel Margoliash, and Henry DI Abarbanel. Dynamical estimation of neuron and network properties i: variational methods. *Biological cybernetics*, 105(3-4):217–237, 2011.

[12] Andreas Wächter and Lorenz T Biegler. On the implementation of an interior-point filter line-search algorithm for large-scale nonlinear programming. *Mathematical programming*, 106(1):25–57, 2006.

[13] J Ye, N Kadakia, PJ Rozdeba, HDI Abarbanel, and JC Quinn. Improved variational methods in statistical data assimilation. *Nonlinear Processes in Geophysics*, 22(2):205–213, 2015.

[14] Jingxin Ye, Daniel Rey, Nirag Kadakia, Michael Eldridge, Uriel I Morone, Paul Rozdeba, Henry DI Abarbanel, and John C Quinn. Systematic variational method for statistical nonlinear state and parameter estimation. *Physical Review E*, 92(5):052901, 2015.